

## Investigation of low temperature dielectric properties of manganese doped-copper oxide nanoparticles by coprecipitation method

H. C. Rao Bitra<sup>a,b</sup>, A. V. Rao<sup>a</sup>, A.G.S. Kumar<sup>b,\*</sup>, G. N. Rao<sup>c</sup>

<sup>a</sup>Advanced Functional Materials Research Centre, Department of Physics, KoneruLakshmaiah Education Foundation, Vaddeswaram, AP, 522502, India

<sup>b</sup>Department of Physics, Malla Reddy Engineering College (A), Hyderabad, 500100, Telangana, India

<sup>c</sup>Department of H & S, Marri Laxman Reddy Institute of Technology And Management, Hyderabad, 500043, Telangana, India

Mn-doped CuO nanoparticles were prepared by the co-precipitation method. X-ray diffraction patterns of pristine and Mn-doped CuO (5, 10 and 15%) nanoparticles confirm the formation of monoclinic structure. Scanning electron microscopy revealed that, the change in morphology with increasing Mn content. Dielectric permittivity value increases with increase in Mn concentration. AC conductivity curves depict improvement in conductivity with a low concentration of Mn content. DC conductivity and AC conductivity values are in accordance with Jonscher's universal power law.

(Received May 12, 2021; Accepted September 20, 2021)

**Keywords:** Mn-doped CuO, Dielectric parameters, AC and DC conductivity, Coprecipitation method, CuO nanoparticles

### 1. Introduction

Tiny sized particles are in the order of nano are the main materials for nanotechnology and nanoscience. Technological innovation in nanostructure is a growing and interdisciplinary domain of research and development activity that has captured attention in recent years. In present day researchers focused on the nano sized materials because of its large surface/volume ratio and quantum confinement impacts. High dielectric materials in nano scale particle size attracted much attention and anticipated applications in the microelectronic industry to use as memory devices, capacitors and nano composites[1,2] Transition metal oxide (TMO) materials form the basis of solid-state chemistry for the examining of structure, composition, and several physical and chemical properties[3–5]that are not only of elementary significance but have large industrial applications. A group of TMO forms an ionic solid that can exhibit a large range of optical and electrical properties[6–8]. Some of these materials are as well used in electronic and magnetic apparatus. TMO materials have important applications in the electrolytic process as an electrode[9,10]. Nanostructured transitional metal oxides (TMO) such as SnO, ZnO, TiO, and CuO play a very strategic role in microelectronic devices manufacturing industry such as capacitors, memory devices[11–13], and different organic, liquid crystal devices[14–16]. Copper oxide is a p-type material and its properties can be varied by varying its structure[17]. Our research group synthesized Mn doped CuO to enhance its physical and electrical properties intended for the development and usage in microelectronic devices.

Manganese is more flexible element. It exists in six different states of oxidation. Generally, It is identified either in its reduced +2 state, which is readily dissolved in water, or in the +4 state, which forms numerous kinds of insoluble oxides. Mn<sup>2+/3+</sup> is proven to be an excellent catalyst and has a great impact on dielectric relaxation property. A variety of studies have been performed on mixed oxide catalysts containing copper oxides or manganese oxides. Owing to the outstanding properties of copper oxide nanoparticles, it has been generally exploit in gas sensors, high T<sub>c</sub> superconductors, and photo catalytic solar cells, etc., a variety of techniques are suggested

---

\* Corresponding author: sampathkumar.physics@gmail.com

for the manufacture of nanomaterials of the desired size and properties. The main intention of this work is to synthesize pure CuO and Mn-doped CuO nanoparticles with better quality and purity by the co-precipitation method.

## 2. Experimental

### 2.1. Synthesis:

The Copper (II) nitrate dihydrate ( $\text{Cu}(\text{NO}_3)_2 \cdot 2\text{H}_2\text{O}$ ; Aldrich), Manganese nitrate tetrahydrate ( $\text{Mn}(\text{NO}_3)_2 \cdot 4\text{H}_2\text{O}$ ; Aldrich) were used as precursor materials for the synthesis of pure and Mn-doped CuO nanoparticles by a co-precipitation method. In the synthesis process weighed the amount of copper (II) nitrate dihydrate ( $\text{Cu}(\text{NO}_3)_2 \cdot 2\text{H}_2\text{O}$ ) was dissolved in double distilled water to achieve a 0.1 mole/L solution. For this aqueous copper solution, the NaOH (1M) solution was added drop-wise till pH value reached to  $\sim 11$  at room temperature. The residual blue gel washed number of times with distilled water and that gel was centrifuged and dehydrated in air at  $60^\circ\text{C}$  for 12 hours. This dried gel was annealed in air for 3 hours at  $850^\circ\text{C}$  to decompose the hydrous copper oxide and crystallize it. For the Mn-doped CuO materials, the similar route was adopted with the addition of different concentrations of  $\text{Mn}(\text{NO}_3)_2 \cdot 4\text{H}_2\text{O}$  to Copper nitrate solution.

### 2.2. Characterization Studies:

The structure and purity of the phase of pure and Mn-doped CuO nanoparticles were tested with X-ray Diffraction Powder (XRD) using a Philips diffractometer with  $\text{Cu-K}\alpha$  rays at room temperature. The capacitance (C) and  $\tan\delta$  (dielectric loss tangent) parameters was observed in the frequency range of 20 Hz–1 MHz for temperature ranging from 80 K–350 K with an increment of 5 K by Impedance analyzer and lakeshore temperature controller with a programmed controller. These analyses were carried on a circular, 1mm thick, disk-shaped pellet and a 10mm diameter with silver coated on both sides serving as an electrode.

Using the below equation (1) the real ( $\epsilon'$ ) and imaginary ( $\epsilon''$ ) complex dielectric quantities were computed,

$$\epsilon' = \frac{Ct}{A\epsilon_0} \quad \text{and} \quad \epsilon'' = \epsilon' \tan \delta \quad (1)$$

Where  $\epsilon_0$  the permittivity of the free space ( $\epsilon_0 = 8.854 \times 10^{-12}$  F/m), C corresponds to the capacitance, A is the area of cross-section ( $\text{m}^2$ ), and (t) the thickness of the sample.

## 3. Result and Analysis

### 3.1. Structural Analysis:

Fig.1a depicts the XRD pattern of pristine CuO and Mn-doped CuO of different concentrations (5, 10, and 15%). From the XRD result, it confirms the formation monoclinic structure of Copper Oxide and the peaks match with the JCPDS no. 89-5899[18]. From the spectra some extra peaks marked with (\*) symbol depicts  $\text{CuMn}_2\text{O}_4$ [19] in 10% and 15% with low intensity. Thus, the monoclinic configuration does not change with the doping of the Mn ions in the CuO lattice. It is as well detected that a little shift in peaks positions of Mn-doped CuO nanoparticles towards higher side of the angles ( $\theta$ ) values, indicating a slight distortion in the symmetry of the CuO Structure due to the formation of vacancies and defects in the structure ascribed to substitution of  $\text{Cu}^{2+}$  by  $\text{Mn}^{2+/3+}$ . Khan et al who mentioned that the formation of charge imbalance by Mn doping (i.e.  $\text{Mn}^{3+}$  replacing  $\text{Cu}^{2+}$ )[20] in CuO lattice. The crystallite sizes of the materials were calculated by Scherer's formula[21] in equation 2.

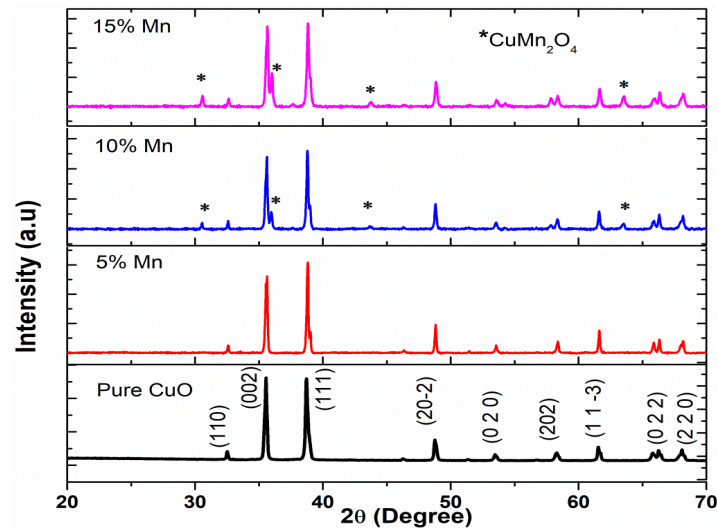


Fig. 1(a) XRD pattern of pure CuO and manganese doped CuO.

$$D = \frac{k\lambda}{\beta \cos\theta} \quad (2)$$

where (D) is the crystallite size, (K) is the dimensionless shape factor (0.9), ( $\lambda$ ) is the X-ray wavelength, ( $\beta$ ) and  $\theta$  are FWHM and Bragg's angle respectively. The reckoned crystallite size of the pure CuO is about 123 nm and Mn-doped CuO were in the range from 44 nm to 65 nm. The lattice parameter and crystallite size values were reduced by doping with Mn, all the reckoned values were entered in table 1.

Table 1. Crystallite size, Lattice parameters and Cell volume of pure CuO and Mn-doped CuO nanoparticles.

Composition	Particle Size (nm)	Lattice Parameter (Å)			Cell Volume (Å <sup>3</sup> )
		A	b	c	
<b>CuO</b>	123.5	4.69680	3.41931	5.11831	81.0731
<b>5%</b>	65.35	4.69666	3.41142	5.10995	80.7285
<b>10%</b>	51.43	4.69792	3.41134	5.1122	80.7943
<b>15%</b>	44.93	4.69503	3.41015	5.10884	80.6625

When Mn content increased beyond 5%, Mn exists in  $Mn^{3+}$  state[19] due to the ionic radius of the difference of  $Mn^{3+}$  0.58Å and  $Cu^{2+}$  is 0.73Å, the crystallite size decrease can be observed which in turn enhanced dielectric properties. Nanoparticles are known to have several surface atoms which have unsaturated in co-ordinations, significant extent of strains are associated with them. The strain ( $\eta$ ) in the lattice of the Mn-doped CuO nanocrystals has been evaluated by the Hall-Williamson relation[22] given below:

$$\beta * \cos(\theta) = \left( \frac{k * \lambda}{D} \right) + \eta * \sin(\theta) \quad (3)$$

where  $\beta$ , is the FWHM of diffraction peaks in radians,  $\theta$  stands for Bragg diffraction angle of the peak,  $\lambda$  is the wavelength of X-rays,  $k$  is the Scherrer constant, and  $D$  crystallite size.  $\beta \cdot \cos(\theta)$  Vs  $\sin(\theta)$  values plotted on graph is shown in Fig.1b. From the graph slope of a straight line acquired for the fitted data reveals the strain value ( $\eta$ ). The strain value is found to be in between 0.001-0.003 for Mn doped CuO nanoparticles.

Fig.2 (a-d) depicts the morphology of pure CuO and Mn-doped CuO nanoparticles. From the figure for 5 %, the Mn-doped images shows nano rod-like structure, 10% and 15% Mn-doped images revealed mixed morphologies of nano flakes assemblies due to the interaction between  $Mn^{2+}$  ions and  $Cu^{2+}$  oxide nanoparticles.

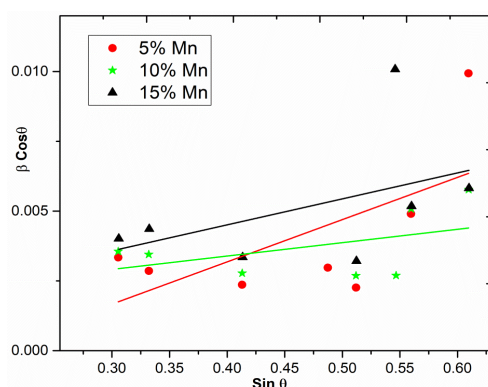


Fig. 1 (b). William-Hall plot for strain in the samples.

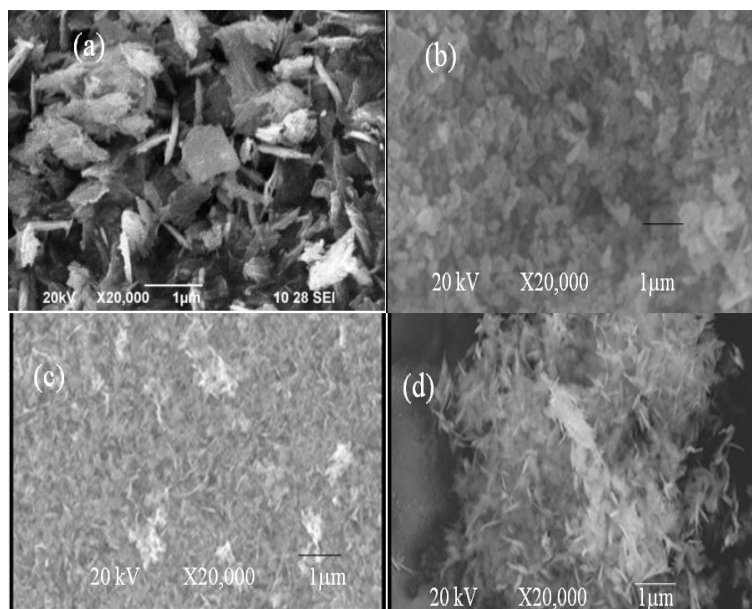


Fig. 2. SEM micrographs of (a) pure CuO; (b) 5% Mn doped CuO; (c) 10% Mn doped CuO; (d) 15% Mn doped CuO.

### 3.2. Dielectric properties

#### 3.2.1. Dielectric permittivity

The dielectric measurements of the Mn-doped CuO material studied by LCR meter were depicted in the Fig.3 (Real part of Dielectric Permittivity ( $\epsilon'$ ) Vs Temperature (T)). From the figure the curves of  $\epsilon'(T)$  for all pure and Mn-doped CuO particles were not dependent on frequency in

addition to temperature <100 K. So, calculated intrinsic static dielectric constant assessments are 2.25, 2.96, and 5.5 for 5%Mn, 10%Mn, and 15% Mn dopant fractions respectively. If the temperature rises above 100 K, the dielectric permittivity increases linearly, independent of temperature and frequency.

It is also clear after the figure that there is a linear variation of the dielectric constant to the temperature. Due to thermal relaxation, we observed low permittivity value at low temperatures, and the permittivity value increases concerning temperature due to the thermal excitation of atoms[23,24]. From the figure, the permittivity value of the pure CuO is about >10,000. And its permittivity value decreases to >50 for copper oxide doped with Mn nanoparticles because the permittivity value depends on the dimension of the particle which was reported earlier by Kharazzi et.al[25,26], and also the CuO grain and grain boundary effects permittivity value but in the case of Mn doped CuO value the grain and grain boundary effects were less and also the Mn was a Magnetic material. Mn-doped CuO permittivity varies in a small fraction concerning the doping concentration[27], here we observe that the variation due to the presence of the Mn<sup>2+</sup> and Mn<sup>3+</sup> ions in the Cu<sup>2+</sup> ions lattice. As we know that dielectric polarizability is directly proportional to the cube root of the ionic radius which leads to a decrease in dielectric polarizability value for higher doping values [28]. The polarization mechanism explained with help of Maxwell – Wagner theory of interfacial polarization in equation[29] (4):

$$\text{Tan}\delta = \frac{\epsilon'}{\epsilon''} \quad (4)$$

From Fig.4 we detected that the dielectric loss peak varies inconsistent (Debye relaxation peaks) with the temperature. This behavior is explained based on the Rezlescu model[30]. Conferring to this model Debye peaks formed due to combined role of p-type and n-type charge carriers, here p-type charges hopping of holes between Mn<sup>2+</sup> and Mn<sup>3+</sup> while the n-type electrons Cu<sup>2+</sup> and Cu<sup>3+</sup> ions in the lattice. The dielectric loss values shift towards high frequency direction with increase in temperature corresponding to relaxation phenomenon. With increasing doping concentration this relaxation phenomenon decreases indicating effect of Mn doping. The Tangent loss vs T graph shows a peak at each temperature with increase in magnitude indicates thermal contribution in losses. Now the activation value can be estimated form the peak position (T<sub>p</sub>) of Tanδ vs T plot using Arrhenius relation.

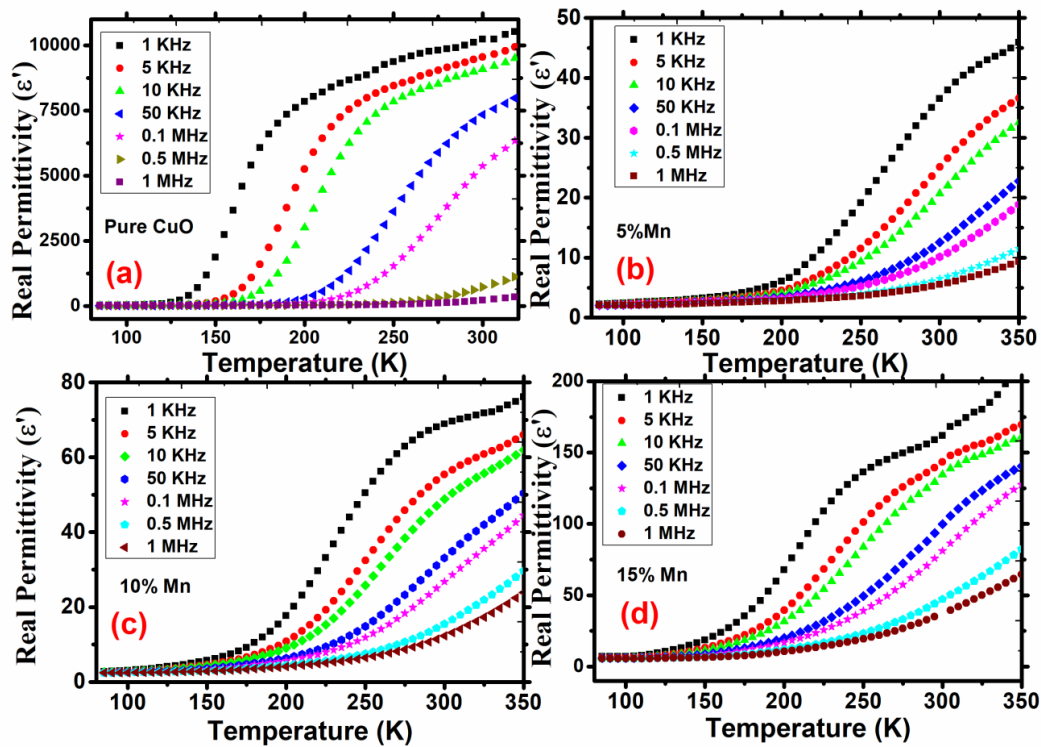


Fig. 3 Dielectric permittivity as a function of temperature at different frequencies (1K-1MHz) of Mn doped CuO nanoparticles a) Pure CuO, b) 5% Mn, c) 10%Mn & d) 15% Mn, respectively.

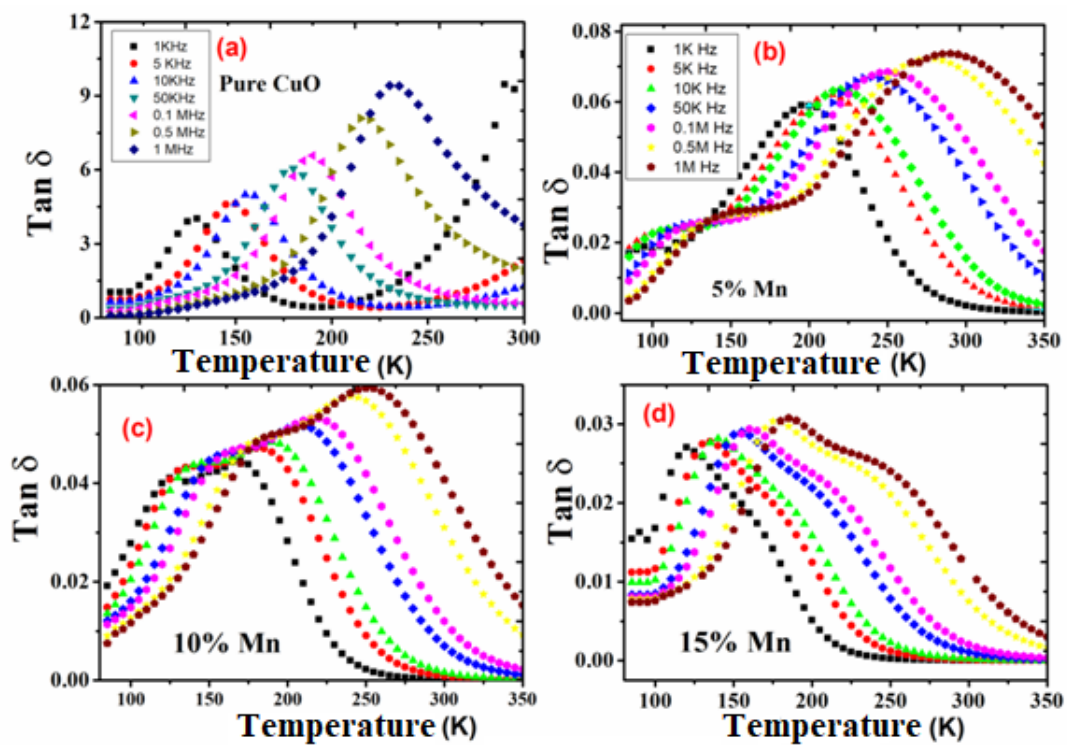
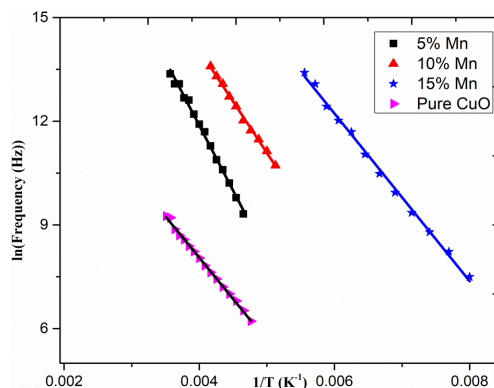


Fig. 4. Dielectric loss factor ( $Tan \delta$ ) as a function of temperature ( $T$ ) at different frequencies (a) Pure, (b) 5%, (c) 10% and (d) 15% Mn) doped CuO nanoparticles.

Now the data fit with the Arrhenius relation, shown in Fig.5. The activation energies were measured using the following equation (5),

$$f = f_0 \exp(E_a / K_B T_p) \quad (5)$$



**Fig. 5.** Frequency vs  $1/T$  plot for 5%, 10%, 15% Mn doped CuO and pure CuO materials and the curve fitted to the Arrhenius equation.

where  $f_0$  is the pre-exponential term,  $E_a$  is the activation energy and  $K_B$  is the Boltzmann constant. The graph among frequency and reciprocal of temperature shown in Fig.5, fit with Arrhenius equation. The derived fitting parameters are  $E_a = 0.31$  eV and  $f_0 = 2.51 \times 10^{11}$  Hz for 5%,  $E_a = 0.24$  eV and  $f_0 = 1.51 \times 10^{10}$  Hz for 10%,  $E_a = 0.12$  eV and  $f_0 = 3.04 \times 10^9$  Hz for 15%.

### 3.2.2. Electric Modulus

Frequency-dependent electric modulus plots of the copper oxide doped with manganese samples in the temperature range from 80 K to 300 K were depicted in Fig.6. The electrical module denotes theoretically to the relaxation of the electrical field in the substance, such that the electrical segment describes the real dielectric relaxation, this indicates in the next equations

$$M^* = M' + i M'' \quad (6)$$

$$M^* = \frac{1}{\epsilon^*} = \frac{\epsilon'}{\epsilon'^2 + \epsilon''^2} + i \frac{\epsilon''}{\epsilon'^2 + \epsilon''^2} \quad (7)$$

where  $M'$  is real electric modulus and  $M''$  as imaginary electric modulus components.

The complex modulus also gives the information about (i) the electrical response of the materials to understand the relaxation occurrence in ionic conductors and ceramic materials, (ii) clarifies the grain as well as grain boundary effects arising at high temperatures which may not be distinct from complex impedance plots. The complex electrical module has been discussed with both permittivity and impedance to research and inspect the contribution of the grain boundary to the material relaxation process, as well as providing us with opportunities to investigate microscopically long-range conduction and localized dielectric relaxation phenomenon [31–36]. From the figure all curves showing almost semicircles at low frequency region with almost lower values [37] attributing to grain boundary effect. With increasing Mn concentration the grain interior and grain boundary well separated. It is also perceived that the 10% Mn-doped sample shows the formation of the grain periphery whereas 5% and 15% show the formation of grains.

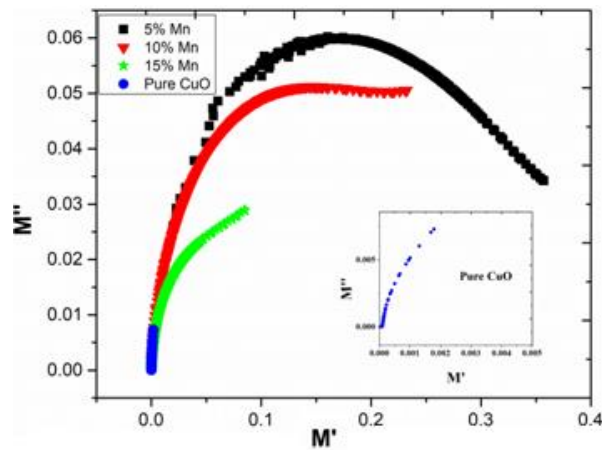


**Fig. 6.** Variation of  $M''$  with real part  $M'$  of the electric modulus and ambient temperature of 5%, 10%, and 15% Mn-doped CuO (inset pure CuO).

### 3.2.3. AC Conductivity

The electrical properties of the pure and Mn-doped CuO materials estimated by AC conductivity were shown in Fig.7. It depends on the applied frequency, temperature, and hopping model[38,39]. The conductive mechanism explained based on the Jonscher's universal power law [40,41].

$$\sigma_{ac}(\omega) = \sigma_{dc} + A\omega^n \quad (8)$$

Here A is temperature-dependent constant,  $\omega$  is frequency exponent ( $n < 1$ ) depend on temperature. This frequency exponent value determines the type of conduction mechanism.

From the above equation 'n' value is independent of temperature which gives quantum mechanical tunneling and large polaron tunneling for the value 'n' is small and increase with rise in temperature and the 'n' value decrease with temperature it could be explained basing on CBH (Correlated Barrier Hopping) model. From the figure, it is experiential that the conduction mechanism is a hopping model, and the AC conductivity of the 5% and 10% Mn-doped CuO values increases because of  $\text{Cu}^{2+}$  replaces with  $\text{Mn}^{2+}$  which leads to an increase AC conductivity value whereas 15% Mn doped sample value decreases because of interchange of  $\text{Mn}^{2+}$  with  $\text{Mn}^{3+}$ . For 15% Mn-doped CuO the reduction in the hopping mechanism is due to the barrier caused by the isolation of a significant number of defects and vacancies at the grain boundary in the context of higher doping. The same feature observed effect of grain boundary barrier formation of Ni and Mn-doped  $\text{Sn}_2\text{O}$ [42].

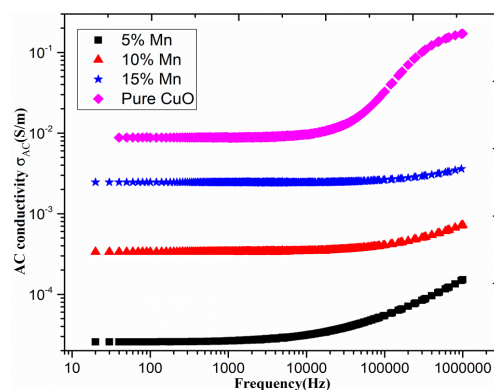


**Fig. 7.** The frequency dependent ac conductivity ( $\delta_{ac}$ ) at room temperature for 5%, 10%, 15% Mn doped CuO and pure CuO nanoparticles.

### 3.3. DC Conductivity

Fig.8 depicts the DC conductivity mechanism plotted the graph  $\sigma_{DC}$  vs  $1000/T$  and fitting the data with Arrhenius equation:

$$\sigma_{DC} = \sigma_0 \exp(-EA/k_B T) \quad (9)$$

where  $E_A$  is the activation energy,  $\sigma_0$  is the pre-exponential factor and  $k_B$  is Boltzmann's constant, and  $T$  is temperature. DC conductive mechanism comprehended well with the pre-exponential factor. The activation energy is estimated on the slope of the  $\sigma_{DC}$  vs.  $1000/T$  plot. The obtained activation energies for Mn-doped materials are  $E_A = 0.35$  eV (5%),  $0.34$  eV (10%) and  $0.3$  eV (15%). The measured activation energies  $E_a$  for loss factor is close to the DC conduction which indicates dielectric polarization and electrical conduction mechanism is matching in the samples.

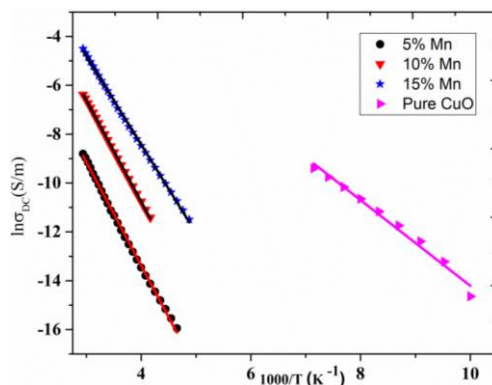


Fig. 8. The DC conductivity ( $\sigma_{DC}$ ) vs  $1000/T$  for 5%, 10%, 15% Mn doped CuO and pure CuO nanoparticles.

## 4. Conclusions

Copper Oxide doped with Manganese Nanoparticles were synthesized by co-precipitation method and annealed at temperature  $850^\circ\text{C}$ . Powder X-ray diffraction patterns be evidence of the structure of Copper Oxide and Mn doped CuO nanoparticles possessed monoclinic structure. The micro-strain values  $0.001$ - $0.003$  calculated from the Williamson-Hall graph were found to be less than the reported values. The dielectric constant and dielectric loss values found to stand less at higher frequencies showed that these materials are appropriate for application in microelectronic devices. AC conductivity values are improved with a small amount of Mn doping in CuO and decrease with increase Mn content indicating particles exhibiting the hopping mechanism.

## Acknowledgments

The authors (B. Hema Chandra Rao and A. Venkateswara Rao) would like to thank the management of KLEF, Department of Science and Technology (DST), Govt. of India, for the award of the DST-FIST level-I (SR/FST/PS-I/2018/35) scheme to Department of Physics and Principal and Management of Malla Reddy Engineering College (Autonomous) for providing facilities.

## References

- [1] P. Thomas, A. Ashokbabu, R. S. Ernest Ravindran, R. Vaish, IEEE Trans. Dielectr. Electr. Insul. 26(2), 568 (2019).
- [2] R. Kumar, R. K. Chaudhary, Radioengineering 27(2), 391 (2019).
- [3] S. S. Sastry, L. T. Kumar, T. Vishwam, V. R. K. Murthy, S. Lakshminaryana, H. S. Tiong,

- Adv. Condens. Matter Phys. 2014, (2014).
- [4] A. GuruSampath Kumar, X. Li, Y. Du, Y. Geng, X. Hong, Appl. Surf. Sci. 509, (2020).
- [5] A. GuruSampath Kumar, L. Xuejin, Y. Du, Y. Geng, X. Hong, J. Alloys Compd. 798, 467 (2019).
- [6] A. Shahat, M. R. Awual, M. Naushad, Chem. Eng. J. 271(Ii), 155 (2015).
- [7] N. Senthilkumar, M. Ganapathy, A. Arulraj, M. Meena, M. Vimalan, I. Vetha Potheher, J. Alloys Compd. 750, 171 (2018).
- [8] S. K. S. Basha, G. S. Sundari, K. V. Kumar, M. C. Rao, Polym. Bull. 75(3), 925 (2018).
- [9] M. Maddaiah, A. G. Kumar, L. Obulapathi, T. S. Sarmash, K. C. Babu Naidu, D. J. Rani, T. S. Rao, Dig. J. Nanomater. Biostructures 10(1), 155 (2015).
- [10] S. K. Pendyala, K. Thyagarajan, A. GuruSampath Kumar, L. Obulapathi, J. Aust. Ceram. Soc. 54(3), 467 (2018).
- [11] S. Sarkar, P. K. Jana, B. K. Chaudhuri, H. Sakata, Appl. Phys. Lett. 89 (May 2013), 212905 (2006).
- [12] V.S. Samyuktha, A.G.sampath Kumar, T.S. Rao, R.P. Suvarna, Digest J. Nanomater. Biostructures. 16(3) 839-846 (2021).
- [13] P. Thongbai, T. Yamwong, S. Maensiri, J. Appl. Phys. 104(7), 0 (2008).
- [14] D. Das, S. Babu, N. Ouerfelli, J. Mol. Liq. 266, 62 (2018).
- [15] K.V. Botlagunta M, Kamma S, Mallampalli B, Biointerface Res. Appl. Chem. 8(3), 3335 (2018).
- [16] V. Sharon Samyuktha, A. Guru Sampath Kumar, T. Subba Rao, R. Padma Suvarna, Materials Today: Proceedings 3(6), 1768 (2016).
- [17] H. Chandra Rao Bitra, A. V. Rao, K. S. Babu, G. N. Rao, Mater. Chem. Phys. 254(June), 123379 (2020).
- [18] Z. Li, Y. Li, H. Zhou, Z. Wang, Digest J. Nanomater. Biostructures. 15(2) 459-464 (2020),
- [19] G. N. Rao, Y. D. Yao, J. W. Chen, J. Appl. Phys. 101(9), 2005 (2007).
- [20] I. Khan, S. Khan, H. Ahmed, R. Nongjai, AIP Conf. Proc. 1536, 241 (2013).
- [21] A. Gurusampath Kumar, T. S. Sarmash, D. J. Rani, L. Obulapathi, G. V. V. B. Rao, T. S. Rao, K. Asokan, J. Alloys Compd. 665, 86 (2016).
- [22] G. K. Williamson, W. H. Hall, Acta Metall. 1(1), 22 (1953).
- [23] A. Dennis Raj, M. Jeeva, R. Purusothaman, G. Venkatesa Prabhu, M. Vimalan, I. Vetha Potheher, J. Mater. Sci. Mater. Electron. 28(11), 7802 (2017).
- [24] D. J. Rani, A. G. S. Kumar, L. Obulapathi, T. S. Rao, IEEE Trans. Dielectr. Electr. Insul. 26(4), 1134 (2019).
- [25] S. Kharrazi, D. C. Kundaliya, S. W. Gosavi, S. K. Kulkarni, T. Venkatesan, S. B. Ogale, J. Urban, S. Park, S. W. Cheong, Solid State Commun. 138(8), 395 (2006).
- [26] M. D. Parvez Ahmad, A. Venkateswara Rao, K. Suresh Babu, G. Narsinga Rao, Mater. Chem. Phys. 224, 79 (2019).
- [27] M. D. Parvez Ahmad, A. Venkateswara Rao, K. Suresh Babu, G. Narsinga Rao, J. Adv. Dielectr. 10(4), (2020).
- [28] T. Munir, M. Sharif, H. Ali, M. Kashif, A. Sohail, N. Sabir, N. Amin, A. Mahamood, N.Ahmed, Digest J. Nanomater. Biostructures. 14(2) 279-284 (2019),
- [29] S. K. Pendyala, K. Thyagarajan, A. Gurusampath Kumar, L. Obulapathi, J. Microw. Power Electromagn. Energy 53(1),1-7 (2019).
- [30] N. Rezlescu, E. Rezlescu, Phys. Status Solidi 23(2), 575 (1974).
- [31] V. F. Lvovich, Impedance Spectroscopy: Applications to Electrochemical and Dielectric Phenomena (John Wiley and Sons, 2012).
- [32] P. Chandra Sati, M. Kumar, S. Chhoker, Ceram. Int. 41(2), 3227 (2015).
- [33] P. Gogoi, P. Srinivas, P. Sharma, D. Pamu, J. Electron. Mater. 45(2), 899 (2016).
- [34] Z. Cao, X. Liu, W. He, X. Ruan, Y. Gao, J. Liu, Phys. B Condens. Matter 477, 8 (2015).
- [35] I. Coondoo, N. Panwar, A. Tomar, A. K. Jha, S. K. Agarwal, Phys. B Condens. Matter 407(24), 4712 (2012).
- [36] S. Karadaş, S. A. Yerişkin, M. Balbaş, Y. Azizian-Kalandaragh, J. Phys. Chem. Solids 148(September 2020), (2021).
- [37] R. Lefi, F. Ben Nasr, H. Hrichi, H. Guerhazi, Optik (Stuttg). 127(13), 5534 (2016).

- [38] H. Saghrouni, S. Jomni, W. Belgacem, N. Hamdaoui, L. Beji, *Phys. B Condens. Matter* 444, 58 (2014).
- [39] R. S. E. Ravindran, P. Thomas, S. Renganathan, *Bull. Mater. Sci.* 42(1), (2019).
- [40] F. Yakuphanoglu, Y. Aydogdu, U. Schatzschneider, E. Rentschler, *Solid State Commun.* 128(2–3), 63 (2003).
- [41] J. Ashok, N. Purnachand, J. Suresh Kumar, M. Srinivasa Reddy, B. Suresh, M. P. F. Graça, N. Veeraiah, *J. Alloys Compd.* 696(2017), 1260 (2017).
- [42] Y. Xu, Y. Geng, L. Wang, A.G. Sampath Kumar, L. Fang, Y. Du and X. Li, *J. Phys. D: Appl. Phys.* 51, 285104 (2018).